Universiteit Leiden
The Netherlands

In vivo Raman spectroscopy for bladder cancer detection using a superficial Raman probe compared to a nonsuperficial Raman probe

Stomp-Agenant, M.; Dijk, T. van; Onur, S.; Grimbergen, M.; Melick, H. van; Jonges, T.; ... ; Swol, C. van

Citation
Stomp-Agenant, M., Dijk, T. van, Onur, S., Grimbergen, M., Melick, H. van, Jonges, T., ... Swol, C. van. (2022). In vivo Raman spectroscopy for bladder cancer detection using a superficial Raman probe compared to a nonsuperficial Raman probe. *Journal Of Biophotonics*, *15*(6). doi:10.1002/jbio.202100354

Version:	Publisher's Version
License:	Creative Commons CC BY-NC 4.0 license
Downloaded from:	https://hdl.handle.net/1887/3666107

Note: To cite this publication please use the final published version (if applicable).

Check for updates

Received: 16 November 2021 | Revised: 21 January 2022 | Accepted: 16 February 2022

DOI: 10.1002/jbio.202100354

RESEARCH ARTICLE

JOURNAL OF BIOPHOTONICS

In vivo Raman spectroscopy for bladder cancer detection using a superficial Raman probe compared to a nonsuperficial Raman probe

Michelle Stomp-Agenant[1,2*] | **Thomas van Dijk**[2] | **Alexander R. Onur**[2] | **Matthijs Grimbergen**[2] | **Harm van Melick**[3] | **Trudy Jonges**[4] | **Ruud Bosch**[5] | **Christiaan van Swol**[2]

[1]Department of Urology, Leiden University Medical Center, Leiden, The Netherlands

[2]Department of Medical Physics, St. Antonius Hospital, Nieuwegein, The Netherlands

[3]Department of Urology, St. Antonius Hospital, Nieuwegein, The Netherlands

[4]Department of Pathology, University Medical Center Utrecht, Utrecht, The Netherlands

[5]Department of Urology, University Medical Center Utrecht, Utrecht, The Netherlands

***Correspondence**
Michelle Stomp-Agenant, Department of Medical Physics, St. Antonius Hospital, Nieuwegein, The Netherlands.
Email: michelleagenant@gmail.com

Abstract

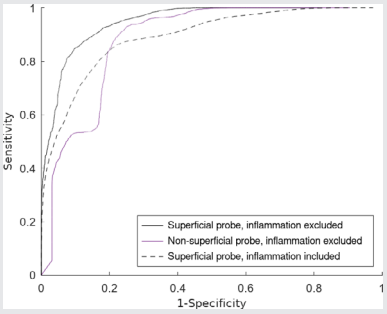

Raman spectroscopy is promising as a noninvasive tool for cancer diagnosis. A superficial Raman probe might improve the classification of bladder cancer, because information is gained solely from the diseased tissue and irrelevant information from deeper layers is omitted. We compared Raman measurements of a superficial to a nonsuperficial probe, in bladder cancer diagnosis. Two-hundred sixteen Raman measurements and biopsies were taken in vivo from at least one suspicious and one unsuspicious bladder location in 104 patients. A Raman classification model was constructed based on histopathology, using a principal-component fed linear-discriminant-analysis and leave-one-person-out cross-validation. The diagnostic ability measured in area under the receiver operating characteristics curve was 0.95 and 0.80, the sensitivity was 90% and 85% and the specificity was 87% and 88% for the superficial and the nonsuperficial probe, respectively. We found inflammation to be a confounder and additionally we found a gradual transition from benign to low-grade to high-grade urothelial carcinoma. Raman spectroscopy provides additional information to histopathology and the diagnostic value using a superficial probe.

KEYWORDS

bladder cancer, Raman, Raman probe, spectroscopy, urology, urothelial carcinoma

This is an open access article under the terms of the Creative Commons Attribution-NonCommercial License, which permits use, distribution and reproduction in any medium, provided the original work is properly cited and is not used for commercial purposes.
© 2022 The Authors. *Journal of Biophotonics* published by Wiley-VCH GmbH.

1 | INTRODUCTION

Bladder cancer is the 10th most common malignancy worldwide [1, 2], and urothelial carcinoma is the most prominent subtype.

Generally, the detection of bladder cancer is performed using white light cystoscopy, which has a limited sensitivity (62%–82%) and specificity (43%–98%) [3–5].

Subsequently, transurethral resection of a bladder tumor (TURBT) using white light cystoscopy is performed for pathologic assessment, but it is also therapeutic. Because recurrence and progression rates are high, up to 55% after nonmuscle-invasive bladder cancer (NMIBC) resection, patients are being exposed to an extensive follow-up program [6]. Recurrence and progression could result from tumor residual after incomplete resection, or from malignant tissue that was not recognized as such, as occurs with flat lesions like carcinoma in situ (CIS). To improve urothelial carcinoma detection and to avoid residual tumor after resection, novel diagnostic techniques are being investigated and some have been recently implemented.

Photodynamic diagnosis (fluorescence cystoscopy) has been introduced supplementing white light cystoscopy during TURBT. This optical technique enhances the contrast between benign and malignant tissue using violet-blue light after preoperative instillation of the bladder with a photosensitive dye. Photodynamic diagnosis has a sensitivity of 92%, compared to 71% of white light cystoscopy alone [7]. This technique offers improved tumor detection, resulting in reduced residual tumor rates after TURBT and superior detection of CIS compared to white light cystoscopy.

However, photodynamic diagnosis has a limited specificity that leads to up to 26% false positive biopsies [7]. This results in unnecessary tissue resection, stress to the patient with a burden of unnecessary care and corresponding complications. Therefore, a more specific diagnostic optical technique could improve the overall diagnostic value.

Raman spectroscopy is a well-established, highly specific optical technique that allows biochemical cancer diagnosis in various organs, without removing any tissue [8–15]. This technique is based on an inelastic interaction of monochromatic light photons with molecular bonds of biological tissue. As a consequence, the scattered photons are frequency-shifted. The frequency shift depends on the particular molecular bond that the photons interact with. By obtaining a spectrum of these frequency-shifted photons, a distinct biochemical fingerprint is acquired. It makes label free biochemical identification possible.

There are several publications describing Raman spectroscopy in bladder cancer diagnosis [16–18]. Chen et al. showed that it is possible to identify and characterize bladder cancer by a fiber-optic Raman probe ex vivo in 32 bladder tissue samples [19].

Our group previously reported results of using a Raman system in vivo during clinical practice for bladder cancer diagnosis [20, 21]. We used a nonsuperficial Raman probe, which collected spectra from multiple tissue layers, that is, high volume, and reached a sensitivity of 85% and specificity of 79% [10]. It was hypothesized that the sensitivity and specificity for bladder cancer detection and grading ability would increase if a superficial Raman probe would be used, because information is gained solely from interaction of photons in the superficial diseased tissue and irrelevant information from deeper layers is omitted. Ideally, the sampled volume should match the volume of the investigated tissue layer. Therefore, a measuring depth of 0–200 μm would be adequate for NMIBC diagnosis, as the thickness of benign urothelial tissue is three to seven cell layers thick (100–200 μm) covering an underlying stromal tissue layer that yields minimal information. In a phantom study, we demonstrated the feasibility of a clinical superficial Raman probe with a measuring depth of 0–200 μm [22]. Other groups also have published results on confocal Raman probes [23, 24].

In this study, we calculated the area under the receiver operating characteristic curve (AUROCC), sensitivity and specificity of urothelial carcinoma detection and grading in vivo, using the superficial probe measurements compared to the nonsuperficial probe measurements with the Raman setup used in the previous study [10]. We also present the in vivo signal-to-noise ratio differences of these probes. Furthermore, we investigate the confounding influence on the classification of inflammation of the tissue. Finally, we present the gradual progression from benign to low-grade and high-grade in the principal component space.

2 | MATERIALS AND METHODS

Data collection was conducted at the St. Antonius Hospital, the Netherlands. Ethical approval was obtained to perform in vivo Raman measurements from suspicious bladder lesions and locations not suspect for malignancy before biopsy/resection (MREC UMC Utrecht). Informed consent was obtained from all patients. The data processing algorithms were developed in GNU octave version 6.1.0 [25].

2.1 | Patient inclusion

Patients of at least 18 years old with a scheduled TURBT were included after informed consent, from March 2013 to December 2014. Patients with excessive hematuria, which hindered direct visualization of lesions during the procedure, were excluded.

18640648, 2022, 6, Downloaded from https://onlinelibrary.wiley.com/doi/10.1002/jbio.202100354 by University Of Leiden, Wiley Online Library on [08/12/2023]. See the Terms and Conditions (https://onlinelibrary.wiley.com/terms-and-conditions) on Wiley Online Library for rules of use; OA articles are governed by the applicable Creative Commons License

Sixty six new patients (156 unique biopsy sites) were included in this study alongside 38 patients (60 unique biopsy sites) from the dataset of Draga et al. [10].

2.2 | Raman system

The used Raman system has been described by Draga et al. [10]. The system consists of a 785-nm diode laser (DFB-0785-1000, Sacher Lasertechnik, Marburg, Germany), a spectrograph (HoloSpec Imaging Spectrograph *fl*1.8i [HSG-785-LF], Kaiser Optical Systems, Ecully, France), a charge-coupled device camera (PIXIS 256 BRDD, Princeton Instruments, Trenton, New Jersey, USA), a personal computer and a superficial and nonsuperficial probe (EmVision LLC, Loxahatchee, Florida, USA) that have been described by Agenant et al. [22]. The nonsuperficial Raman probe is a standard fiber bundle style probe with collection fibers surrounding an excitation fiber. The superficial probe uses the same external dimensions; however, to enable sampling of a superficial layer, an overlap of focus of the excitation beam and collection region is created by a convergent lens as shown in Figure 1.

2.3 | Raman spectroscopy procedures

In the operating room, a white light cystoscopy was performed and the location and number of lesions was determined. Subsequently, a Raman measurement and a tissue biopsy of one to four locations suspect for malignancy were performed as well as from one normal appearing location from the posterior bladder wall.

During the procedure, the Raman probe and the biopsy forceps were advanced parallel to each other through an angled cystoscope, into the bladder. After minimizing the ambient light and disconnecting the light cable, the Raman probe was placed in gentle contact to the lesion for a Raman measurement (10 consecutive spectra with an acquisition time of 500 ms each). After this, the light cable was reconnected and a corresponding biopsy was taken. Each biopsy was separately fixated in formalin and sent for pathology analysis as in standard care.

After the patient left the operating room, the calibration measurements were performed in the same lighting conditions as the in vivo measurements.

All biopsies were evaluated using the WHO 2004 classification system for malignancy grading of bladder cancer, by a pathologist specialized in uro-oncology (G. N. Jonges).

2.4 | Spectra exclusion and preprocessing

Spectra of biopsy samples that could not be classified by the pathologist due to limited or damaged tissue were excluded. Some spectra were excluded due to the saturation of the CCD camera. After excluding these spectra, 5–10 spectra were included per biopsy location. Depending on the number of remaining spectra, there was

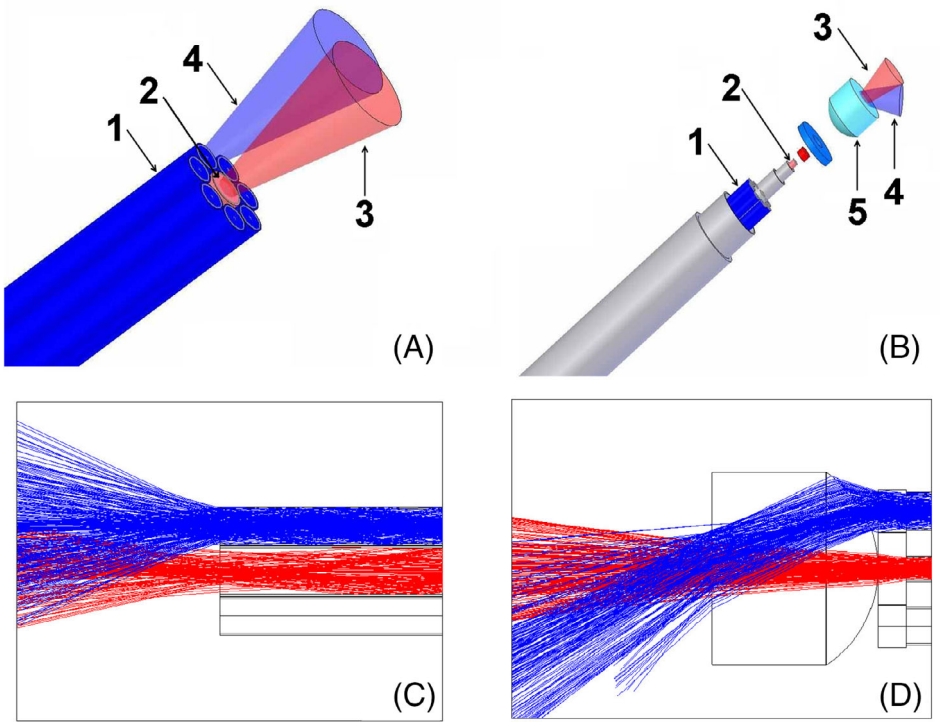

FIGURE 1 Top left (A) and right (B) are exploded views of the distal probe tip of the nonsuperficial and superficial Raman probe with a sampling depth of 300 and 200 μm, respectively. The Raman laser excitation region and the direction of the Raman collection cone(s) create an overlap with the laser cone at the surface of the lens and is illustrated for the nonsuperficial Raman probe (A) and the superficial Raman probe (B). (1—collection fibers, 2—excitation fiber, 3—Raman laser cone, 4—Raman collection cone and 5—convergent lens). Bottom left (C) and right (D) are Zemax traces by EMVISION of the nonsuperficial and superficial Raman probe using the refractive index of water, respectively (for more details, see reference [22])

18640648, 2022, 6, Downloaded from https://onlinelibrary.wiley.com/doi/10.1002/jbio.202100354 by University Of Leiden, Wiley Online Library on [08/12/2023]. See the Terms and Conditions (https://onlinelibrary.wiley.com/terms-and-conditions) on Wiley Online Library for rules of use; OA articles are governed by the applicable Creative Commons License

a difference in acquisition time. To correct for this inequality in total acquisition time, the spectra per biopsy specimen were summed and divided by their total acquisition time. The Raman signal was collected in the 400–1800 cm^{-1} spectral region with a spectral resolution of 4 cm^{-1}.

Using Raman measurements of specific calibration substances, the spectra were calibrated: spectral dispersion of the detection system was corrected using a neon-argon light and standardization of the Raman shift axis was performed using acetaminophen.

The following preprocessing steps were executed in order:

1. Calibrate wavelengths
2. Reject overexposed spectra
3. Sum spectra at each tissue sample/biopsy
4. Separate noise with Savitzky–Golay filter (order 3, frame length 13)
5. Normalize measurement by exposure time
6. Subtract autofluorescence [26]
7. Divide by total autofluorescence
8. Perform extended multiplicative scatter correction [27]

2.5 | Signal-to-noise ratio

To determine signal-to-noise ratio, we separated the measured spectrum in a Raman signal component and a noise component (step 4 of preprocessing). First, we obtained the Raman signal by applying a digital filter to smooth the measurement data (Savitzky–Golay filter, order 3, width 13 points, or 18.2 wavenumbers). Then, we took the noise to be the absolute value of the difference between this Raman component and the measured spectrum. For a given spectrum, we defined the signal-to-noise ratio as the sum over wavenumbers of the Raman signal, divided by the sum over wavenumbers of the noise. We have verified that the noise obtained in this manner is proportional to the square root of the fluorescence signal, which is the characteristic of photon shot noise. To compare SNR between measurements with differing acquisition times, we made a correction by dividing by the square root of the acquisition time.

2.6 | Classification

For the classification, we excluded all biopsies that contained inflammation to enable comparison to the dataset of Draga et al., as we only had access to the biopsies of Draga et al. that do not contain inflammation.

The preprocessed data were used to train a diagnostic classification model. The diagnostic classification model was based on the principal-component fed linear-discriminant-analysis (PCA/LDA) as described by Crow et al. [9]. To reduce the class imbalance, synthetic minority oversampling technique (SMOTE) was applied [28]. A classification is an average over 10 runs with SMOTE. A leave-one-person-out cross-validation model was used. As a performance metric, the AUROCC is reported. The number of principal components was obtained by optimizing the AUROCC. Using the optimized number of principal components, we repeated the classification 100 times. This resulted in a mean and standard deviation of the sensitivity and specificity and AUROCC as performance metrics, generated from 100 confusion matrices.

3 | RESULTS AND DISCUSSION

3.1 | Patient characteristics

Spectra were taken from 156 unique biopsy locations, in 66 patients. The patient and pathologic characteristics are described in Table 1 and are equally distributed in each pathology groups. Due to saturation, 15 of the 1560 spectra were excluded, which resulted in 1445 spectra of 156 biopsy locations.

We excluded biopsies that contained inflammation according to the histopathologic analysis resulting in 57 noninflamed biopsies and performed the same five preprocessing steps and analysis on their data [10].

3.2 | Signal-to-noise ratio

The median signal-to-noise ratio of all Raman spectra (benign and malignant together, including inflammation) for the superficial probe was 12.5, compared to 6.5 for the nonsuperficial probe, an increase with a factor 1.92 (Figure 2).

3.3 | Classification

The average spectra of the three pathological groups are presented in Figure 3. Specific band intensities that differed between pathology groups are more clearly shown in Figure 4. This figure presents the difference spectra of two of the three determined pathology groups. Figures 3 and 4 show bands that might be able to distinguish benign from malignant tissue, such as at 492, 1082, 1264, 1304 and 1444 cm^{-1}. Also, high-grade urothelial carcinoma could be distinguished from benign or low-grade urothelial carcinoma, for example, at the 1656-cm^{-1} band, which might be valuable in the classifier to

18640648, 2022, 6, Downloaded from https://onlinelibrary.wiley.com/doi/10.1002/jbio.202100354 by University Of Leiden, Wiley Online Library on [08/12/2023]. See the Terms and Conditions (https://onlinelibrary.wiley.com/terms-and-conditions) on Wiley Online Library for rules of use; OA articles are governed by the applicable Creative Commons License

TABLE 1 Patient and pathology characteristics

Patient parameters	Superficial probe data set	Superficial probe data set excluding inflammation	Nonsuperficial data set
Number of included patients	66	37	38
Number of biopsies/Raman measurements	156	57	60
Mean age (years)	64.6	64.8	70
Pathology groups			
Benign	109	38	28
Benign not suspect for malignancy	58	29	-
Benign suspect for malignancy	51	9	-
Malignancy	47	19	32
Low-grade malignancy	25	11	-
High-grade malignancy + CIS	17 + 5	8	-

Note: In the nonsuperficial data set, information about tumor grade and whether the tissue was suspected for malignancy was not documented and is therefore absent.
Abbreviation: CIS, carcinoma in situ.

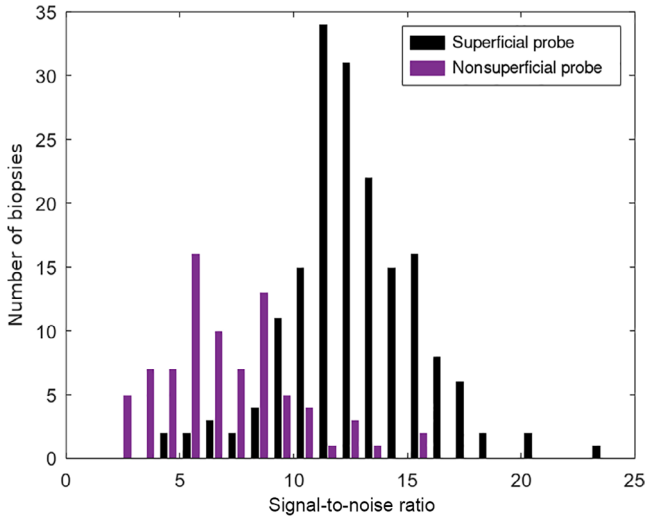

FIGURE 2 Histogram of signal-to-noise ratio of the superficial and nonsuperficial probe. The determined signal-to-noise ratios are set against the number of Raman spectra (after preprocessing)

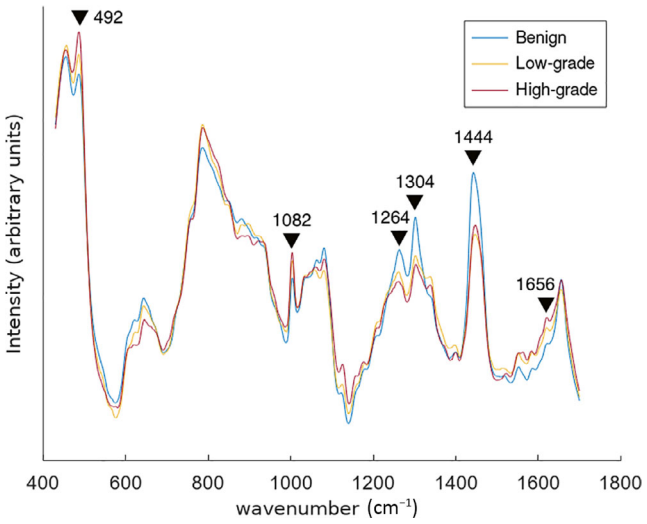

FIGURE 3 Mean Raman spectra of each pathology group of the superficial probe (inflammation excluded)

distinguish the three pathology groups from each other. Nevertheless, the difference between low-grade and high-grade urothelial carcinoma is limited as shown in Figure 4.

3.4 | Analysis

After the preprocessing, PCA was implemented for dimensional reduction of the datasets of the superficial and nonsuperficial Raman probes, separately.

Our dataset consisted of superficial Raman spectra of 156 biopsy locations. The dataset from the previous study (Draga et al.) consisted of nonsuperficial Raman spectra of 60 biopsy locations that were dimensionally reduced using principal components. The number of principal components was chosen to optimize the AUROCC of the classification model per measurement set to enable probe comparing.

The confusion matrices after the linear discriminant analysis and the leave-one-person-out cross-validation of both probes are presented in Table 2. The sensitivity, specificity and AUROCC were 90% (± 4%), 87% (± 4%) and 0.95 (± 0.01) for the superficial probe and 80%

18640648, 2022, 6, Downloaded from https://onlinelibrary.wiley.com/doi/10.1002/jbio.202100354 by University Of Leiden, Wiley Online Library on [08/12/2023]. See the Terms and Conditions (https://onlinelibrary.wiley.com/terms-and-conditions) on Wiley Online Library for rules of use; OA articles are governed by the applicable Creative Commons License

(± 2%), 85% (± 3%) and 0.88 (± 0.01), for the nonsuperficial probe, respectively. The number of principal components necessary to optimize the AUROCC was 18 for the nonsuperficial probe and 10 for the superficial probe. For correct comparison of our clinical study to the clinical study of Draga et al., the same exclusion criteria and preprocessing was used on both data sets. As a consequence, slightly different values are reported compared to the ones published by Draga et al. [10].

Figure 5 presents the ROC curve of the superficial and nonsuperficial Raman probe (compared to Random 1). The area under the curve of the superficial and nonsuperficial probe is 0.95 and 0.88, respectively. This indicates that the performance of the superficial probe is better than the nonsuperficial probe. In addition, the ROC curve of the superficial probe with inflammation in the biopsy is shown. In this situation, the performance of the probe is reduced which could be explained by different Raman signals that will be obtained from an inflamed biopsy location, as a range of different cells that will be present in an ongoing inflammation. Nevertheless, as inflammatory cells will be present as a reaction of the immune system to a tumor, this might be unavoidable and it would be better to include the inflamed biopsy locations. Maybe, the amount of inflammation could be prognostic for the progression of the tumor or the response to immune therapy, which is under development by others. More research will be needed to evaluate this.

Finally, we performed the PCA-LDA analysis with leave-one-out cross-validation for the three pathology groups; benign, low-grade and high-grade urothelial carcinoma. In this analysis, only two PCs were used. The confusion matrix is listed in Table 3 and the total accuracy was

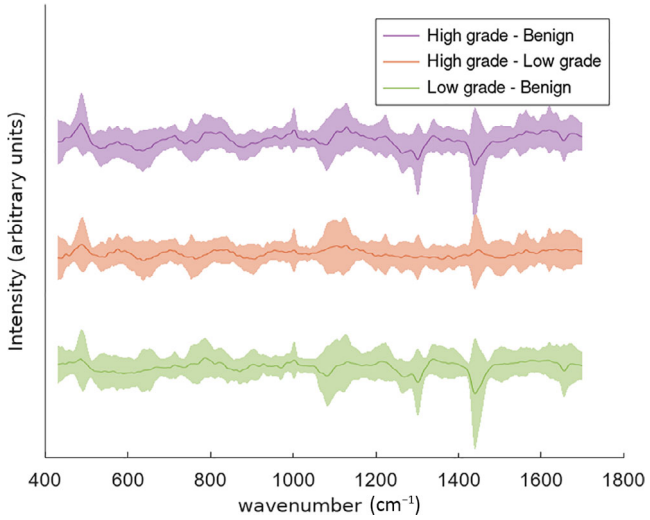

FIGURE 4 Difference of mean spectra and the standard deviation between every two pathology groups (inflammation excluded): (green) low-grade minus benign, (orange) high-grade minus low-grade and (purple) high-grade minus benign

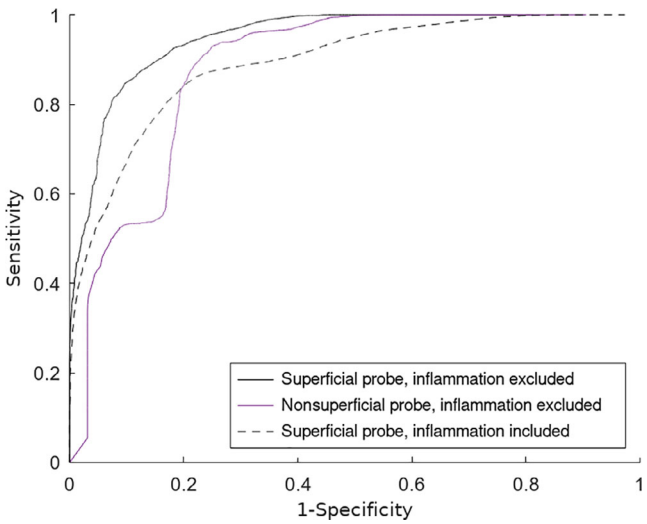

FIGURE 5 Receiver operating characteristic (ROC) curve of the diagnostic accuracy for the superficial and nonsuperficial Raman probe

TABLE 2 Mean and standard deviation over 100 confusion matrices using the optimized number of PCs for leave-one-person-out cross-validation of logistic regression-based Raman decision algorithm compared to the histopathologic assessment which is the "gold standard" describing benign and malignant tissue for the superficial probe and the nonsuperficial probe, excluding inflamed biopsies

			Histopathology ("gold standard")	
			Malignant	**Benign**
Raman spectroscopy	Superficial probe	Malignant	17.2 ± 0.7	5.1 ± 1.4
		Benign	1.8 ± 0.7	32.9 ± 1.4
		AUROCC: 0.95 ± 0.01	Sensitivity: 90% ± 4%	Specificity: 87% ± 4%
	Nonsuperficial probe	Malignant	25.5 ± 0.6	4.1 ± 0.9
		Benign	6.5 ± 0.6	23.9 ± 0.9
		AUROCC:0.88 ± 0.01	Sensitivity:80% ± 2%	Specificity:85% ± 3%

18640648, 2022, 6, Downloaded from https://onlinelibrary.wiley.com/doi/10.1002/jbio.202100354 by University Of Leiden, Wiley Online Library on [08/12/2023]. See the Terms and Conditions (https://onlinelibrary.wiley.com/terms-and-conditions) on Wiley Online Library for rules of use; OA articles are governed by the applicable Creative Commons License

TABLE 3 Confusion matrix for leave-one out cross-validation of logistic regression-based Raman decision algorithm compared to the histopathologic assessment which is the "gold standard" describing benign urothelium, low-grade urothelial carcinoma and high-grade urothelial carcinoma, resulting in an accuracy of 59%

		Histopathology ("gold standard")		
		Benign	**Low-grade**	**High-grade**
Raman spectroscopy	Benign	22.3 (59.0)	1.2 (3.7)	0.7 (3.9)
	Low-grade	10.3 (24.7)	5.4 (9.1)	1.3 (4.6)
	High-grade	5.4 (25.3)	4.4 (12.2)	6.0 (13.5)

Note: The numbers are calculated from the database without inflammation, and in parentheses are the numbers including biopsies that contained inflammation.

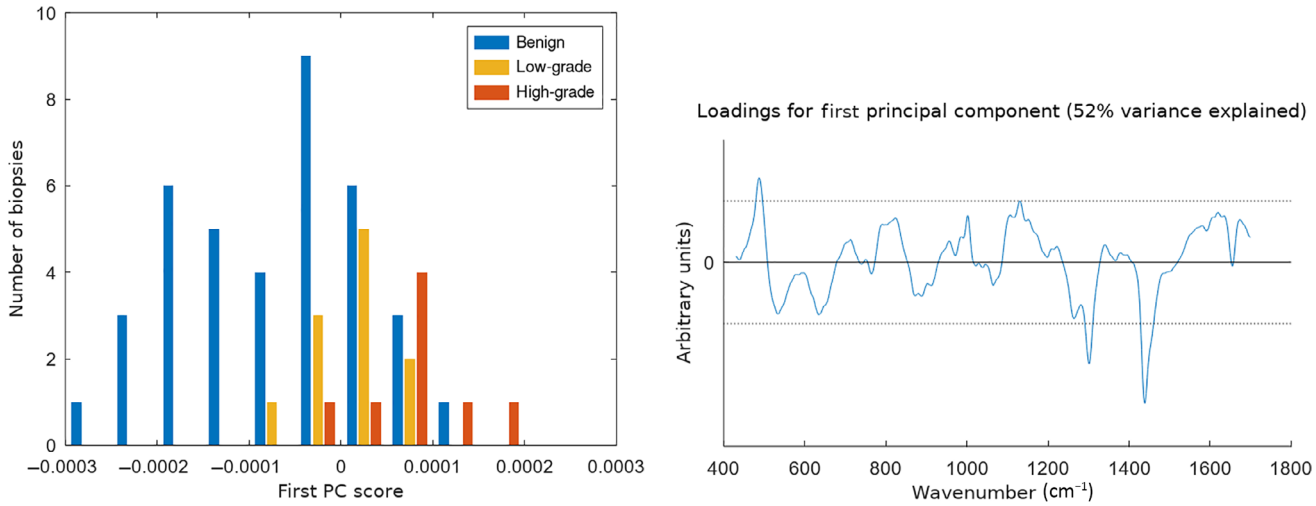

FIGURE 6 The left part shows a histogram, representing the separation of the three classes (excluding inflammation) along the first principal component (for the ternary classification excluding infections). It indicates that progressive evolution from benign to low-grade to high-grade urothelial carcinoma is contained in the Raman spectra. The right part of the figure shows the loadings for the first principal component

63%. The biopsies that contained CIS were limited in number and therefore we combined them with the high-grade urothelial carcinoma because CIS shows high-grade histopathological characteristics.

Unfortunately, it was not possible to compare the probe performance for grading between both probes precisely, as the data of Draga et al. were pathologically assessed using the WHO 1997 grading classification in grades 1, 2 and 3, as opposed to the assessment in the current study, using the 2004 WHO grading classification in low-grade and high-grade urothelial carcinoma.

The limited accuracy is due to the small differences between the low-grade and high-grade urothelial carcinoma spectra that could be explained by the relevant differences, which may cover just a small percentage of the total signal and may therefore not always come to light.

Alternatively, there might be a sampling error in the measurement because only a small volume of the tumor is sampled by the Raman probe. This small volume might not be of the highest grade in the total lesion that has been biopsied because a tumor can be heterogeneous.

Another hypothesis is that the small difference might be explained by a distribution of molecular biochemical characteristics within one pathology group. In our opinion, there is no clear biochemical cutoff value between low-grade and high-grade urothelial carcinoma, but it is probably a continuum of malignant biochemical characteristics that gradually increase when becoming more malignant in the development of urothelial carcinoma. Figure 6 indicates this progressive evolution from benign to low-grade to high-grade urothelial carcinoma. This progressive trend in Raman signal from benign to low-grade to high-grade urothelial carcinoma was also proposed by Chen et al. [19]. If there is a gradual change, this might explain the high inter- and intraobserver variability of the histopathologic assessment [29]. Raman spectroscopy measures quantitative biochemical changes as opposed to the

18640648, 2022, 6, Downloaded from https://onlinelibrary.wiley.com/doi/10.1002/jbio.202100354 by University Of Leiden, Wiley Online Library on [08/12/2023]. See the Terms and Conditions (https://onlinelibrary.wiley.com/terms-and-conditions) on Wiley Online Library for rules of use; OA articles are governed by the applicable Creative Commons License

histopathologic analysis, which assesses morphologic and histopathologic differences. Maybe the poor reproducibility of the histopathologic analysis could be solved using Raman spectroscopy. To empower this hypothesis, future research should be performed using Raman spectroscopy in a higher resolution and larger data set to develop an improved diagnostic algorithm.

4 | CONCLUSION

This study investigated the in vivo clinical potential of our superficial probe in diagnosis of NMIBC.

The signal-to-noise ratio was improved with a factor 1.92, compared to the nonsuperficial probe, used by Draga et al. [10]. This is a confirmation our group's earlier phantom model results with this new probe [22].

The sensitivity, specificity and AUROCC were 90%, 87% and 0.95 for the superficial probe and 80%, 85% and 0.88, for the nonsuperficial probe, respectively, in discriminating benign from malignant tissue. Therefore, the performance of the superficial probe is superior to the nonsuperficial probe. This might be due to the improved signal-to-noise ratio. However, we think that the decreased measuring depth of the probe is also responsible, as the tissue information is solely from the diseased depth and deeper unaffected tissue do not cloud the result. We have not been able to quantify this yet. As a next step, it would be interesting to link our Raman shift findings at specific wavenumbers and to its biochemical bonds where the Raman signals originate from.

We also found an indication that there exists a progressive evolution from benign to low-grade to high-grade UC.

Tissue inflammation leads to a worse classification performance, but it cannot be excluded as the immune system responds with inflammation to tumor development.

Further research needs to be performed to differentiate low-grade from high-grade urothelial carcinoma. In our opinion, the transition between benign, low-grade and high-grade urothelial carcinoma in different patients should be evaluated with a higher spatial resolution, for example, ex vivo in cystectomy specimens over a grid of locations, generating a larger data set. This will provide us with more information about the biochemical nature of the malignancy leading to an improved diagnostic algorithm for Raman spectroscopy.

ACKNOWLEDGMENTS

The authors thank Eric Marple for probe production and Olivier Wegelin for measuring Raman spectra.

DATA AVAILABILITY STATEMENT

The data that support the findings of this study are available on request from the corresponding author. The data are not publicly available due to privacy or ethical restrictions.

ORCID

Michelle Stomp-Agenant https://orcid.org/0000-0001-9010-1339

REFERENCES

[1] S. Antoni, J. Ferlay, I. Soerjomataram, A. Znaor, A. Jemal, F. Bray, *Eur. Urol.* **2017**, *71*(1), 96.

[2] M. G. K. Cumberbatch, I. Jubber, P. C. Black, F. Esperto, J. D. Figueroa, A. M. Kamat, L. Kiemeney, Y. Lotan, K. Pang, D. T. Silverman, A. Znaor, J. W. F. Catto, *Eur. Urol.* **2018**, *74*(6), 784.

[3] O. Brunckhorst, Q. J. Ong, D. Elson, E. Mayer, *Surg. Endosc.* **2019**, *33*, 1349.

[4] C. C. Cauberg Evelyne, J. J. M. C. H. de la Rosette, T. M. de Reijke, *Indian J. Urol.* **2011**, *27*(2), 245.

[5] D. Jocham, H. Stepp, R. Waidelich, *Eur. Urol.* **2008**, *53*(6), 1138.

[6] M. Babjuk, M. Burger, E. Comperat, P. Gontero, F. Liedberg, *EAU Guidelines on Non-Muscle-Invasive Bladder Cancer (TaT1 and CIS)*, European Association of Urology, Arnhem **2021**.

[7] M. Rink, M. Babjuk, J. W. F. Catto, P. Jichlinski, S. F. Shariat, A. Stenzl, H. Stepp, D. Zaak, J. A. Witjes, *Eur. Urol.* **2013**, *64*(4), 624.

[8] M. S. Bergholt, W. Zheng, K. Lin, K. Y. Ho, M. Teh, K. G. Yeoh, J. B. Yan So, Z. Huang, *Int. J. Cancer* **2011**, *128*(11), 2673.

[9] P. Crow, J. S. Uff, J. A. Farmer, M. P. Wright, N. Stone, *BJU Int.* **2004**, *93*(9), 1232.

[10] R. O. P. Draga, M. C. M. Grimbergen, P. L. M. Vijverberg, C. F. P. van Swol, T. G. N. Jonges, J. A. Kummer, J. L. H. Ruud Bosch, *Anal. Chem.* **2010**, *82*(14), 5993.

[11] E. M. Kanter, E. Vargis, S. Majumder, M. D. Keller, E. Woeste, G. G. Rao, A. Mahadevan-Jansen, *J. Biophotonics* **2009**, *2*(1–2), 81.

[12] A. Molckovsky, L.-M. W. K. Song, M. G. Shim, N. E. Marcon, B. C. Wilson, *Gastrointest. Endosc.* **2003**, *57*(3), 396.

[13] M. G. Shim, B. C. Wilson, E. Marple, M. Wach, *Appl. Spectrosc.* **1999**, *53*(6), 619.

[14] J. H. Song, I. R. Francis, J. F. Platt, R. H. Cohan, J. Mohsin, S. J. Kielb, M. Korobkin, J. E. Montie, *Radiology* **2001**, *218*(1), 95.

[15] N. Stone, C. Kendall, J. Smith, P. Crow, H. Barr, *Faraday Discuss.* **2004**, *126*, 141, discussion 169–183.

[16] B. W. D. de Jong, T. C. Bakker Schut, K. P. Wolffenbuttel, J. M. Nijman, D. J. Kok, G. J. Puppels, *J. Urol.* **2002**, *168*(4 Pt 2), 1771.

[17] N. Stone, M. C. Hart Prieto, P. Crow, J. Uff, A. W. Ritchie, *Anal. Bioanal. Chem.* **2007**, *387*(5), 1657.

[18] E. Cordero, J. Rüger, D. Marti, A. S. Mondol, T. Hasselager, K. Mogensen, G. G. Hermann, J. Popp, I. W. Schie, *J. Biophotonics* **2020**, *13*(2), e201960025.

[19] H. Chen, X. Li, N. Broderick, Y. Liu, Y. Zhou, J. Han, W. Xu, *J. Biophotonics* **2018**, *11*(9), e201800016.

18640648, 2022, 6, Downloaded from https://onlinelibrary.wiley.com/doi/10.1002/jbio.202100354 by University Of Leiden, Wiley Online Library on [08/12/2023]. See the Terms and Conditions (https://onlinelibrary.wiley.com/terms-and-conditions) on Wiley Online Library for rules of use; OA articles are governed by the applicable Creative Commons License

[20] R. O. P. Draga, M. C. M. Grimbergen, E. T. Kok, T. N. Jonges, C. F. P. van Swol, R. J. L. H. Bosch, *Urol. Int.* **2012**, *89*(3), 326.
[21] M. C. M. Grimbergen, C. F. P. van Swol, R. J. A. van Moorselaar, J. Uff, A. Mahadevan-Jansen, N. Stone, *J. Photochem. Photobiol. B Biol.* **2009**, *95*(3), 170.
[22] M. Agenant, M. Grimbergen, R. Draga, E. Marple, R. Bosch, C. van Swol, *Biomed. Opt. Express* **2014**, *5*(4), 1203.
[23] J. C. C. Day, R. Bennett, B. Smith, C. Kendall, J. Hutchings, G. M. Meaden, C. Born, S. Yu, N. Stone, *Phys. Med. Biol.* **2009**, *54*(23), 7077.
[24] I. Latka, S. Dochow, C. Krafft, B. Dietzek, J. Popp, *Laser Photonics Rev.* **2013**, *7*(5), 698.
[25] J. W. Eaton, D. Bateman, S. Hauberg, R. Wehbring, *GNU Octave Version 6.1.0 Manual: A High-Level Interactive Language for Numerical Computations*, Free Software Foundation, Boston **2020**.
[26] C. A. Lieber, A. Mahadevan-Jansen, *Appl. Spectrosc.* **2003**, *57*(11), 1363.
[27] H. Martens, E. Stark, *J. Pharm. Biomed. Anal.* **1991**, *9*(8), 625.
[28] N. V. Chawla, K. W. Bowyer, L. O. Hall, W. P. Kegelmeyer, *J. Artif. Intell. Res.* **2002**, *16*, 321.
[29] I. Tosoni, U. Wagner, G. Sauter, M. Egloff, H. Knönagel, G. Alund, F. Bannwart, M. J. Mihatsch, T. C. Gasser, R. Maurer, *BJU Int* **2000**, *85*(1), 48.

How to cite this article: M. Stomp-Agenant, T. van Dijk, A. R. Onur, M. Grimbergen, H. van Melick, T. Jonges, R. Bosch, C. van Swol, *J. Biophotonics* **2022**, *15*(6), e202100354. https://doi.org/10.1002/jbio.202100354

18640648, 2022, 6, Downloaded from https://onlinelibrary.wiley.com/doi/10.1002/jbio.202100354 by University Of Leiden, Wiley Online Library on [08/12/2023]. See the Terms and Conditions (https://onlinelibrary.wiley.com/terms-and-conditions) on Wiley Online Library for rules of use; OA articles are governed by the applicable Creative Commons License